Electron/Jet Separation with the ATLAS detector

P. Pralavorio

CPPM, CNRS/IN2P3 - Univ Mediterranee, Marseille - France

Abstract

Results on the single and inclusive electron reconstruction efficiency as well as the rejection capability against QCD-jets with the ATLAS detector are presented. These studies, based on fully simulated events, include the trigger (first and second level) selection and correspond to low (10^{33} cm^{-2}s^{-1}) and high (10^{34} cm^{-2}s^{-1}) luminosity - in which case pile-up was superimposed. For both luminosities, a jet rejection factor $\geq 10^5$ can be obtained keeping an electron efficiency of $\sim 70\%$.

E-mail: pralavor@cppm.in2p3.fr

1 Introduction

The identification of isolated high-p_T electrons $p_T \geq 20$ (30) GeV at low (high) luminosity will be essential for physics at the LHC, in particular the searches for leptonic decays of the Higgs boson, studies of the production and decay of W's and Z's, the extraction of clean samples of $t\bar{t}$ events for the measurement of m_t as well as electrons for E/p calibration. This note describes the inclusive electron selection and the rejection capability against QCD-jets using information from the Electro-Magnetic(EM) Calorimeter and the Inner Detector(ID).

To obtain an inclusive electron signal, a jet rejection $O(10^5)$ is required (see [1]). To separate electrons from jets, cuts, developed to maintain reasonable electron efficiency even in the presence of pile-up at high luminosity, are based on both the calorimeter detector and the inner tracking systems. Here, a further electron-pion separation can be achieved in particular using Transition Radiation (TR) in the Transition Radiation Tracker (TRT) made of straw tubes.

The note is organised as follows. After a presentation of the tools for ATLAS simulation in section 2, we present the trigger selection applied for first and second level in section 3. In section 4, we extensively present the offline selection and give a summary of results in section 5, including the impact of trigger on the offline analysis. Section 6 is dedicated to conclusions.

2 Detector layout and datasets

The geometry used in this analysis, corresponds to the one described in details in Technical Design Reports (see for the inner detector Ref.[2] and for the Liquid argon calorimeters Ref.[3]). It is described in DICE 98_2, but an older version, DICE 96_12, is also used. The main difference between these two versions concerns:

- The barrel cryostat design (increase of 0.12-0.25 X_0 depending on η in the new version).
- An incorrect digitisation of the transition radiation (TR) in DICE 96_12, which has to be corrected when reading the events (hits are redigitised).

A high statistics sample of around 10^6 fully simulated dijet events with version DICE 96_12 was used [4]. At the parton level, each jet had $p_T > 17$ GeV and was produced within $|\eta| < 2.7$. Initial and final state radiation were simulated. At the same time, other physics processes such as prompt photon production, quark bremsstrahlung, W, Z and top production were generated with the appropriate cross-sections - the complete set of events is referred to as the 'jet sample'. For the efficiency studies, several samples of single electrons were generated with DICE 98_2, $|\eta| < 2.5$ and with fixed p_T of 20 and 30 GeV.

In the following, 'Low luminosity' implies no pile-up. To study the performance at high luminosity, 24 minimum-bias events belonging to the main bunch crossing were superimposed on the electrons and jets [5]. In the electromagnetic calorimeter, the read out time for a single particle is $\sim$ 500 ns and $\sim$ 700 minimum-bias events has been superimposed (and multiplied by the correct weight given by the shaping function). The method used is described in details in [6].

To avoid the processing of events by GEANT [7] that will anyway be rejected by the LVL1 Trigger, datasets have to satisfy the 'particle level filter'[4]: at least one region $\Delta\eta \times \Delta\phi$=0.12$\times$ 0.12 with a summed transverse energy of all stable particles (except muons and neutrinos) greater than 17 GeV.

This results in a jet rejection of 3 (with no efficiency loss for electron). The global jet rejection used in the rest of the analysis will be normalised to the total number of jets passing the particle level filter. These selected events have now to satisfy the trigger conditions.

3 Trigger selection

The ATLAS trigger is organised in three trigger levels (LVL1, LVL2, LVL3), where the first two are simulated in the following. At LVL1, only reduced-granularity information are available from the calorimeters and the muon system, whereas LVL2 uses full-precision data from inner tracking, calorimeters and muon detectors. Electrons and QCD-dijet events were processed by the LVL1 and LVL2 trigger simulation (ATRIG, see [8]).

3.1 LVL1 electron/photon trigger

For the LVL1 trigger the best compromise between electron efficiency and tolerable trigger rate suggests the following criteria (more details can be found in [9]) for low (high) luminosity:

- Transverse energy deposit in the EM calorimeter in 1×2 trigger towers ($\Delta\eta \times \Delta\phi$=0.1×0.1) greater than **16** (**25**) GeV.
- Transverse energy in a ring of 12 trigger towers surrounding the EM cluster less than **2**(**4**) GeV. This criterion insures the shower isolation in the EM calorimeter.
- 16 hadronic trigger towers behind the electromagnetic cluster with a total transverse energy less than **1**(**2**) GeV. This allows to select isolated shower in the hadronic calorimeter.

These criteria were chosen to be efficient for 20 (30) GeV electrons [1]. Each LVL1 object selected with the cuts below are communicated as a Regions-of-interest to the LVL2 trigger.

Figures 1 show the E_T distributions for all clusters found by the reconstruction package ATRECON [10] in the EM Calorimeter for electrons of 30 GeV and dijet events at low and high luminosity after the LVL1 trigger is applied. E_T represents here and in the rest of the analysis the calibrated energy in a cluster of size $\Delta\eta\times\Delta\phi$=0.075×0.125 (in the second sampling of the EM calorimeter this corresponds to 3×5 cells). The entries at low E_T correspond to clusters from low energy particles in the minimum bias events (in the case of pile-up) or particles in the jets themselves; the peaks arise from threshold cuts of around 5 GeV. It is clear that clusters from minimum bias events have low E_T and can be completely removed.

The total jet rejection factor for jets having E_T >17 (25) GeV was approximately 80 (90) for an electron efficiency of about 95%. Only events with showers having a large EM component survived.

3.2 Second Level trigger

The LVL2 electron trigger uses both information from the calorimeter and the inner detector. It allows thus a consequent reduction of the jet contamination and partially overlaps with the selection made in the offline analysis. This aspect will be discussed in details in section 5.

[1] In the low (high) LVL1 luminosity menu this corresponds to single object trigger EM20I (EM30I).

3.2.1 Calorimeter selection, LVL2 Calo

The trigger algorithms for the calorimeter selection of the LVL2 trigger are explained in [9]. Because of a newer version of DICE (98_2 instead of 97_6), and more accurate method to add pile-up events in the EM calorimeter, the cut values, optimised to keep 95 % of electron, have been slightly modified since Ref.[9].

The electron deposited most of his energy in the EM calorimeter and thus the transverse energy deposited in a window of size $\Delta\eta \times \Delta\phi$=0.2×0.2 behind the EM cluster should be very small. Jets can deposit a large fraction of their energy in the hadronic calorimeter, so the following cuts on the hadronic transverse energy are applied for low (high) luminosity:

- $E_T \leq$ **0.45(0.325)** GeV for an EM cluster with $E_T \leq$ 25 GeV.
- $E_T \leq$ **0.6(0.6)** GeV for an EM cluster with 25 GeV $< E_T \leq$ 60 GeV.
- No E_T cut for an EM cluster with $E_T >$ 60 GeV.

Then cuts are applied on the second sampling of the EM calorimeter where most of the electron energy is deposited. Dividing the energy contained in a 3×7 cluster cells ($E_{3\times7}$) by the energy in a 7×7 cluster ($E_{7\times7}$), gives the shower shape in η direction, $R_\eta^{shape}=E_{3\times7}/E_{7\times7}$. This variable should show a peak near R_η^{shape}=1 for the electron because of the very few lateral leakage; large tails at lower values of R_η^{shape} for the jets are expected. Thus:

- $R_\eta^{shape} \geq$ **0.9(0.914)**.

Cuts made in the hadronic and the second sampling of the EM calorimeters reject jets with high energetic pions and wide shower; jets with single or multiple η, π^0, ... are now main contribution which can fake the electrons. In order to reject these jets, the lateral shower shape in the strips can be exploited, where possible. For this, two ϕ-bins are summed and the strip with the largest energy deposit (E_{1st}) is searched in a window $\Delta\eta$=0.125 as well as a second maximum (E_{2nd}). The lateral shower shape can be defined by $R_\eta^{strip}=(E_{1st}-E_{2nd})/(E_{1st}+E_{2nd})$. Because of the absence of an energy-significant E_{2nd} for the single electrons, $R_\eta^{strip} \sim$1; for the jets with single or multiple η, π^0 the presence of a significantly high second maximum is highly probable. To rejects these candidate, the following cuts are then applied:

- Ratio of the energy deposit in the strips over the EM cluster must be greater than **0.5(0.5)** %.
- $R_\eta^{strip} \geq$ **0.75(0.815)**.

The LVL2 Calorimeter trigger jet rejection factor for jets having E_T >17 (25) GeV was around 5 for an electron efficiency of about 95% at both luminosity. Only events with showers having a large EM component (including π^0, photon conversion, prompt electrons) survived.

3.2.2 Inner Detector selection, LVL2 ID

The trigger algorithms for the inner detector selection of the LVL2 trigger are explained in details in [11]. A dedicated pattern recognition algorithm has been developed and the set of cuts applied on the reconstructed track parameters are as follows:

- In the Semi-Conductor Tracker (SCT): a p_T > **7** (**10**) GeV as well as a matching in position, $|\Delta\eta|$ <**0.15**(**0.3**) and $|\Delta\phi|$ <**0.04**(**0.03**), and in energy, E/p < **3**(**3**), with the EM cluster.
- In the TRT: a p_T > **5**(**5**) GeV and a matching in ϕ position $|\Delta\phi|$ <**0.05**(**0.05**) with the EM cluster.

At this stage, the total jet rejection factor for jets having E_T >17 (25) GeV was around 3500 for an global electron efficiency of about 83%. The events passing the LVL2 calorimeter cuts with showers having a large ($\geq$ 50 %) EM component have been reduced by a factor of 40(20) due to the absence of track reconstructed in the tracker. The corresponding photon conversion events have been reduced by a factor 5(4) because of the absence of track reconstruction for late conversion or wrong track parameters computation for earlier conversions.

In the rest of the analysis, only EM clusters with E_T > 17 (25) GeV at low (high) luminosity were considered. These values correspond to the E_T threshold cut of the single object electron trigger (chosen to be efficient for 20 (30) GeV electrons).

4 Offline Analysis

In order to select electron candidates, the events have to satisfy the offline reconstruction selection and to pass through the LVL1 and LVL2 trigger algorithms. In the following, the calorimeter, ID as well as matching selections of the offline analysis are explained.

4.1 Offline Calorimeter Selection

As it was presented in section 3.2.1, a significant separation between electrons and jets can be achieved by the LVL2 Calorimeter Trigger. Subsequently, the offline calorimeter algorithms can refine the cuts made by the trigger as well as making additional ones.

η	HCAL	2nd sampling		1st sampling				
	E_T(had)/ E_T(em) <	R_η^{shape} >	$\omega_{\eta 2}$ <	ΔE < (GeV)	'ΔE^{max2}' > (GeV)	ω_{tot1} <	ω_1 <	ω_{3s} <
0.00-0.80	f(η)(.04)	.915(.91)	.012(.0115)	.15(.35)	.25(.4)	2.7(3.0)	.35(.34)	.75(.72)
0.80-1.37	.008(.025)	.91(.915)	.012(.012)	.15(.3)	.5(.55)	3.5(3.0)	.60(.45)	.75(.75)
1.37-1.50	.008(.025)	.91(.915)	.012(.012)	–	–	–	–	–
1.50-1.52	.03(.05)	.89(.91)	.012(.012)	–	–	–	–	–
1.52-1.80	.03(.05)	.89(.91)	.012(.012)	.35(.4)	1.1(.7)	3.5(3.0)	.68(.60)	.80(.72)
1.80-2.00	.02(.03)	.92(.92)	.0115(.011)	.2(.8)	.4(1.0)	2.0(2.0)	.30(.25)	.70(.65)
2.00-2.35	.015(.025)	.91(.85)	.0125(.012)	.15(1.0)	.3(1.0)	1.4(1.7)	.20(.18)	.60(.55)
2.35-2.50	.015(.025)	.91(.85)	.0125(.012)	–	–	–	–	–

Table 1: *Cuts applied for the offline Calorimeter selection for low (high) luminosity. The fraction of EM energy in the first sampling must exceed* **0.5***(***0.5***)*%.

A detailed description of the variables, originally introduced for the γ-jet separation and used also for electron/jet selection criteria, can be found in [12]; we will therefore not present extensively, but

rather give general overview, of these variables. The cuts applied in this selection are tuned in such a way that the electron efficiency loss must be less than 2% relative to the LVL2 trigger selection.

The variables used to distinguish high-E_T electrons from jets are:

- Ratio of the transverse energy in the first compartment of the Hadronic Calorimeter, E_T(had), divided by the transverse energy deposit in the EM Calorimeter, E_T(em).
- Ratio of the energy deposited in a 3×7 window divided by the energy deposited in a 7x7 window, R_η^{shape}, in the second compartment of the EM Calorimeter. The Figure 2a) shows the R_η^{shape} distributions for electrons and jets at low luminosity after LVL1 was applied.
- Pseudo-rapidity shower width (energy weighted sum over all cells), $\omega_{\eta 2}$, for a 3×5 cluster in the second compartment of the EM Calorimeter.

To separate the surviving jets from electrons, the very fine granularity in pseudorapidity of the first compartment was exploited by looking for substructures within a shower in pseudo-rapidity and by analysing the overall shower shape - a window of $\Delta\eta \times \Delta\phi = 0.125 \times 0.2$ was used. The electron shower is expected to be narrower with no second maximum compared to the jet which can contain several particles (especially $\pi^0 \to \gamma\gamma$), source of a possible significant second maximum. The variables used to distinguish electrons from jets are (cut values are given in Table 1):

- The fraction of EM energy in the first compartment must exceed $\mathbf{0.5(0.5)}$%.
- The difference between the energy associated with the second maximum (E^{max2}) and the energy deposited in the strip with the minimal value between the first and second maxima(E^{min}), $\Delta E = E^{max2} - E^{min}$. In Figure 2b), distributions of ΔE are shown for electrons and jets at low luminosity (after LVL1 was applied). 'ΔE^{max2}' = $E^{max2}/(1+5(9)\times 10^{-4} E_T(\mathrm{em}))$ had to exceed a given value (see Table 1) to be protected against fluctuations.
- The total shower width in $\Delta\eta \times \Delta\phi = 0.0625 \times 0.2$, ω_{tot1}.
- The shower shape in the shower core, ω_1=[E(±3)-E(±1)]/E(±1), where E(±n) is the energy deposit in ±n strips around the strip with highest energy.
- The shower width using three strips in the shower core, ω_{3s}.

Since the variables are pseudo-rapidity dependent, they were optimised in several intervals to allow for varying granularities, lead thickness and material in front of the calorimeter. The quantities calculated using the first compartment can be used only in the regions $|\eta| < 1.37$ and $1.52 < |\eta| < 2.35$ since there are no strips in $1.4 < |\eta| < 1.5$ nor beyond $|\eta| = 2.4$. The cuts on the variables were tuned in such a way that they were more than 98% efficient for electrons after the LVL1 and LVL2 Triggers. The cut values applied for the offline calorimeter selection can be found in Table 1.

4.2 Inner Detector Selection

After the Calorimeter cuts, the contamination of the inclusive signal from charged hadrons was greatly reduced and the remaining background was dominated by photon conversions and low multiplicity jets

containing high-p_T π^0 mesons. This background was reduced further by requiring the presence of a good ID track pointing to the EM cluster and with a good energy-momentum match.

Tracks were reconstructed with xKalman (see [13]) in a cone of $|\Delta\eta| \times |\Delta\phi| = 0.1 \times 0.1$ around the selected EM clusters, and only tracks with $p_T > 5$ GeV were kept. Where possible, a bremsstrahlung recovery procedure which combine in 3-D the standard track parameters, coming from a fit allowing for multiple scattering, and dE/dx, with the position of the calorimeter cluster centroid, were used. In case of bremsstrahlung recovery procedure is not available (especially for charged pions where the matching between cluster and track is not good), the simple track fit is taken as a measure of the p_T of the track. Among all reconstructed tracks, the one with the highest p_T was required to satisfy the 'extended ID track quality cuts':

- Number of precision (SCT) hits $\geq$ **9** (for 11 at maximum)
- Number of pixel hits $\geq$ **2** (for 3 at maximum)
- Number of B-layer hit = **1** (for 1 at maximum)
- Transverse impact parameter $\leq$ **1**mm
- Number of TRT Straw hits $\geq$ **20** (for $\sim$ 40(50) at maximum in barrel (endcap))

The LVL2 Trigger ensures that there is an associated charged track to the EM cluster within a $|\Delta\eta| \times |\Delta\phi| = 0.1 \times 0.1$ cone, thus removing most of the neutral particles. Hence the jet rejection which was achieved by the offline cuts in the ID was quite small, around 2. The cuts on the number of pixels hits and B-layer were nevertheless still effective against photon conversions, reducing them by a factor of $2 \times 2.5 \sim 5$ at low and high luminosity. Only $3 \pm 3(25 \pm 13)\%$ of the charged hadrons are removed at low (high) luminosity by the extended ID track quality cuts, which are not effective against this contamination.

4.3 Inner Detector/Calorimeter Matching

The jet rejection which was achieved by the cuts in the ID was quite small. This was significantly improved by ensuring consistency between the EM Calorimeter and ID information. Firstly the angular matching between the track and the EM cluster was checked, allowing for the track curvature and the vertex position (the variables defined below are the same as the one used for electron/photon separation [14]):

- $\Delta\eta = \eta_{CALO}^{strips} - \eta_{TRACK}$; η_{CALO}^{strips} is computed in the strips of the EM calorimeter with a correction for the spread of the primary vertex in z, and η_{TRACK} is the extrapolation of the track pseudo-rapidity down to the primary vertex.
- $\Delta\phi = \phi_{CALO}^{2nd} - \phi_{TRACK}$, ϕ_{CALO}^{2nd} is computed in the second sampling of the EM calorimeter and takes into account the track curvature in ϕ.

Distributions for the absolute value of these two variables are shown in Figure 3. They are obtained after the LVL2 Trigger is applied (rather than after the ID cuts) so as to increase the statistics in the plots. In both distributions the prompt electrons clearly peak at 0 while charged hadrons and conversions show tails at higher values because of an incorrect position matching. It was required that:

- $|\Delta\eta| < \mathbf{0.01}$ **(0.02)**
- $|\Delta\phi| < \mathbf{0.02}$

at low (high) luminosity.

Subsequently, the energies measured by the two sub detectors were compared - see Figure 4. At low (high) luminosity, it is required that:

- **0.7 (0.6)** $<$ E/p $<$ **1.4**.

The tail at low values of E/p for conversion electrons arises when one photon from a π^0 converts and the second photon was included in the EM cluster causing the track fit (incorporating the calorimeter bremsstrahlung recovery procedure) to overestimate the momentum.

An extra factor of ~ 2 can be obtained from these cuts keeping a high electron efficiency (around 98%). It should be noted that the track fit procedure (bremsstrahlung recovery procedure) partially overlap with the Inner Detector/Calorimeter matching because both use calorimeter cluster centroid position. Therefore it is more relevant to consider the product of both rejection factors, which is about 4.2 at low and high luminosity.

4.4 Use of Transition Radiation in the TRT

The jets which survived the selection procedure described so far consisted mainly of signal electrons. At low luminosity, where the E_T cuts is at 17 GeV, 80% came from heavy flavour and 20% from W's and Z's; at high luminosity, the E_T cut rises to 25 GeV and the fractions became 20% and 80% respectively. The fraction of e-like jets arising from the mis-identification of charged hadron backgrounds was 30% (40%) of the jets at low (high) luminosity. The fraction of e-like jets coming from photon conversions was greatly reduced by the previous cuts.

The emission of transition radiation (TR) photons in the straw tubes of the TRT is a threshold effect proportional to the inverse of the mass (more precisely on $\gamma =$ E/m). The separation between electrons and pions is effective for E$<$100 GeV and vanished after because the rate of TR photons emitted by pions and electrons are comparable. A further reduction of the charged hadron contamination is thus obtained by rejecting tracks having a low fraction of TRT straws with a high-threshold TR hit[2]. The cuts applied are arranged in p_T bins (0:0.75, 0.75:1.5, 1.5:3.5, 3.5:12.5, 12.5:30, $>$ 30 GeV) and η bins (0.25 step). They are tuned to obtain 90% electron efficiency ('loose transition radiation cuts') at both low and high luminosity (see Section 3.4.1 of Ref.[15]). With the available jet statistics the hadrons candidates are reduced from 17 (6) to 0 (1) at low (high) luminosity, consistent with expectations.

5 Summary of Results

In the studies reported here, the jet rejection has been normalised to the total number of jets with $E_T > 17$ GeV, smeared and reconstructed at the particle-level using ATLFAST (see [16]). This is believed to give an estimate of the jet rejection which can be achieved by ATLAS which is more

[2]For example for 12.5 GeV$<$ p_T $<$ 30 GeV and 0.25$<$ η $<$ 0.50, tracks must have more than 14.2% of straws with a high-threshold TR hit.

meaningful for comparisons with theoretical predictions. This normalisation results in a jet rejection which is a factor of three lower than would be obtained with no E_T cut applied at the parton level.

Cuts	Low Luminosity			High Luminosity	
	Eff e20 (%)	Eff e30 (%)	Rej jets (10^3)	Eff e30 (%)	Rej jets (10^3)
LVL1	94.0	99.0	0.08±0.001	96.1	0.09±0.001
LVL2 Calo	90.5 (96.3)	96.9 (97.8)	0.39±0.01 (4.9±0.1)	92.1 (95.6)	0.48±0.02 (5.2±0.2)
LVL2 ID	82.5 (91.1)	87.9 (90.7)	3.5±0.3 (8.9±0.6)	82.5 (89.5)	3.7±0.5 (7.8±0.9)
Offline Calo	80.9 (98.1)	86.8 (98.6)	9.8±1.2 (2.8±0.3)	81.1 (98.3)	8.4±1.5 (2.2±0.3)
Offline ID	77.4 (93.8)	83.0 (94.5)	16.8±2.7 (1.7±0.2)	77.2 (93.6)	22.7±6.9 (2.7±0.7)
Matching	75.4 (97.5)	79.5 (95.7)	40±10 (2.4±0.5)	75.3 (97.4)	35.8±13 (1.6±0.4)
TR	68.5 (90.8)	72.7 (91.4)	>150	67.5 (89.7)	>45

Table 2: *Effect of different sets of cuts on electron efficiencies (p_T = 20 and 30 GeV) and jet rejections (E_T > 17 GeV and $|\eta|$ < 2.5). The cuts are described in more detail in the text. The numbers shown are the effect of the cumulative cuts, with the relative changes (percent or absolute numbers) shown in brackets.*

Summaries for low and high luminosity of the electron efficiencies compared to the jet rejections resulting from the succession of cuts applied and in different pseudo-rapidity intervals are given in Tables 2 and 3 respectively. The electron efficiencies are determined from the high-statistics electron samples, while the jet rejection is calculated from the reductions in the jet sample but with the signal electrons explicitly excluded. To normalise the jet rejection, only jets with E_T > 17 (25) GeV have been considered at low (high) luminosity. The final jet rejections correspond to 1 (2) events at low (high) luminosity and the values in Table 2 correspond to 90% confidence limits calculated according to the prescription in [17]. The event that passes all cuts at low luminosity is a 50 GeV electron coming from a photon conversion in the barrel (η=0.5). No attempt has been made to reject this event with the conversion reconstruction [18]. At high luminosity, the same event is kept (the 'jet sample' used at high luminosity is the one used at low luminosity on which pile-up has been superimposed), as well as a second event with a EM cluster of E_T=30 GeV in the barrel and a pointing hadron coming from a π^0.

Pseudo-rapidity	Low Luminosity		High Luminosity
	Eff e20 (%)	Eff e30 (%)	Eff e30 (%)
0.0 - 0.7	74.7± 1.3	75.0± 1.4	70.6± 1.6
0.7 - 1.37	68.0± 1.4	72.6± 1.4	68.4± 1.7
1.37 - 1.52	45.3± 3.3	49.0± 3.4	40.4± 3.9
1.52 - 2.0	64.3± 1.7	75.2± 1.7	65.1± 2.1
2.0 - 2.5	71.6± 1.6	74.3± 1.7	72.8± 2.1

Table 3: *Electron efficiencies (p_T = 20 and 30 GeV) after all cuts as a function of pseudo-rapidity.*

In Figure 5, the E_T distribution of candidates in the jet sample is shown at low and high luminosity

at various stage of the offline analysis. The exact composition of the jets after each step of the analysis is given in Table 4.

Cuts	$\gamma \rightarrow e^+e^-$ (%)	Hadrons (%)	Electrons (%)
LVL1+LVL2	27±3(25±5)	40±4(53±5)	33±4(18±4)
Offline Calo	32±4(45±8)	29±4(30±7)	39±5(25±7)
Offline ID	10±3(10±7)	39±6(45±11)	51±6(45±11)
Matching	2±2(6±6)	28±6(38±12)	70±6(56±12)
TR	3±3(9±9)	0(9±9)	97±3(82±12)

Table 4: *Composition of QCD-dijet events for different sets of cuts at low (high) luminosity. The numbers shown are given in % and with respect to all jets with E_T >17(25) GeV.*

With the cuts described in this section, it was possible to achieve an overall electron efficiency for p_T = 20 GeV (30 GeV) of 68.6% (72.7%) at low luminosity. The addition of pile-up decreased the efficiency for the 30 GeV electrons down to 67.5%, which is comparable to what was achieved at low luminosity for 20 GeV electrons. A corresponding jet rejection of the order of 10^5 was obtained at both low and high luminosity. Compared to the tabulated results (in particular, Tables 6-2 and 6-4 in the ID TDR [2]), the electron efficiency has fallen by 20% mainly because of the explicit application of the transition radiation (TR) cuts (loss of 10%), the simulation of the trigger (see next paragraph), as well as tighter Inner Detector cuts. In the later case, the main changes come from a smaller cone search (0.1×0.1 instead of 0.3×0.2), harder ID SCT cuts (Number of pixel hits $\geq$ 2 instead of 1, and 1 B layer hit – this cut was not present before) as well as better quality of TRT track (number of TRT $\geq$ 20 – this cut was not present before). This mainly results in rejecting electrons from photon conversion (a factor 6 is gained). Consequently the jet rejection has increased by a factor 50 mainly because of the TR cuts and the improved calorimeter and ID cuts.

The trigger losses are shown in Table 5 and can be broken down as follows: 2.3% (5.6%) due to the ID cuts in LVL2, 1.5% (1.5%) due to the calorimeter cuts in LVL2 and 2% (3%) in LVL1 at low (high) luminosity. Figures 6 and 7 shows the electron cluster E_T distribution and the electron efficiency versus η distribution at low and high luminosity for various sets of cuts (LVL1+LVL2+Reco, LVL1+Reco, Reco). One can clearly see from Figure 6 that the lowest part of the E_T spectrum is the most affected by the full chain analysis, partly because of the trigger cuts (this is especially true for p_T=20 GeV). There is thus a room for improvement by adjusting the LVL2 trigger cuts to approach the offline ones.

The selection procedure outlined above lead to a signal (inclusive electrons) to background (charged hadrons and conversions) of more than 20 (5) for low (high) luminosity, although large uncertainties remain on the cross-sections for the different processes. The electron efficiency was cross-checked by considering the signal electrons in the inclusive jet sample; however, since the fraction of events with electrons in the sample was very small, the statistical errors are large. For electrons coming from W/Z decays, the efficiency was 54±13% (60±15%) and for those coming from b and c semi-leptonic decays, it is 14±2.5% (3.4±2.4%) for low (high) luminosity.

Cuts	Low Luminosity		High Luminosity
	Eff e20 (%)	Eff e30 (%)	Eff e30 (%)
LVL1+LVL2+Reco	68.6	72.7	67.5
LVL1+LVL2 Calo+LVL2 SCT+Reco	69.5	73.8	69.5
LVL1+LVL2 Calo+Reco	70.2	75.2	71.3
LVL1+Reco	71.4	75.6	72.4
Reco	73.6	75.9	74.0

Table 5: *Effect of various trigger cuts on the global electron efficiency at low and high luminosity. The numbers shown are given in %. 'Reco' means all the offline cuts.*

6 Conclusions

This note presents the e/jet separation power of the ATLAS detector. For the first time, the study was based on a full simulation of the complete chain of cuts from LVL1 trigger to the offline analysis, for both low and high luminosity.

The electron identification takes profit of the transverse and longitudinal segmentation of the EM calorimeter as well as high precision silicon tracker and the transition radiation functionality of the TRT. The EM calorimeter is very powerful to reject hadrons even after LVL1 and LVL2 trigger cuts are applied (keeping 95 % efficiency, one can reject hadrons by a factor greater than 10). The ID allows to reduce significantly the neutral hadrons, electrons from photons conversions and charged hadrons (using the transition radiation photons emitted in the TRT).

The jet sample was analysed to demonstrate that the signal electrons could be extracted from the background. At both luminosity, a jet rejection factor $\geq 10^5$ can be obtained keeping a ≥ 70 % electron efficiency. Finally, the trigger losses are estimated to 2.3% (5.6%) at low (high) luminosity. These losses should be studied in details to maximise the overlap between LVL2 trigger and offline cuts.

Acknowledgements

I would like to thank Monika Wielers for constant support and help to interface the trigger selection and Stephen Haywood for fruitful discussions. Special thanks to Sasha Rozanov for carefully reading this manuscript.

References

[1] T. Pal et al., *Inclusive electron identification and QCD-jet rejection in the ATLAS detector*, ATL-INDET-96-127.

[2] ATLAS Collaboration, *ATLAS Inner Detector Technical Design Report*, CERN/LHCC/97-16.

[3] ATLAS Collaboration, *ATLAS Liquid Argon Calorimeter Technical Design Report*, CERN/LHCC/96-41.

[4] A. Dell'Acqua et all., *1997 ATLAS jet production*, ATL-PHYS-97-102.

[5] M. Wielers, *Procedure to add Pile-up in the Inner Detectors and the Calorimeters at design Luminosity*, http://home.cern.ch/~wielers/pileup.ps.gz

[6] S. Simion, *Pile-up Simulation for Atlas Calorimeters*, ATL-COM-SOFT-99-001.

[7] R. Brun et al., *GEANT-CERN Program Library*, W5013, October 1994.

[8] ATLAS ATRIG Working Group, *ATRIG version 3.00*, http://home.cern.ch/~hansl/atrig.ps

[9] ATLAS Collaboration, *Trigger Performance Status Report*, CERN/LHCC/98-11.

[10] J. Schwindling, *The reconstruction code for the electromagnetic calorimeter in ATRECON*, http://atlasinfo.cern.ch/Atlas/GROUPS/PHYSICS/EGAMMA/emreco973.ps

[11] J.T.M. Baines et al., *Identification of high p_T electrons by the Second Level Trigger of ATLAS*, ATL-COM-DAQ-99-007.

[12] M. Wielers, *Photon Identification with the ATLAS detector*, ATL-COM-PHYS-99-011.

[13] I. Gavrilenko, *Description of Global Pattern Recognition Program (xKalman)*, ATL-INDET-97-165.

See also http://atlasinfo.cern.ch/Atlas/GROUPS/INNER_DETECTOR/LAYOUT/DOC/kalman.ps

[14] D. Rousseau, *Electron/photon separation*, ATL-PHYS-98-119.

[15] ATLAS Collaboration, *ATLAS Detector and Physics Performance*, CERN/LHCC/99-14.

[16] E. Richter-Was, D. Froidevaux, L. Poggioli, *ATLFAST 2.0 a fast simulation package for ATLAS*, ATL-PHYS-98-131.

[17] Particle Data Group, Particle Physics Booklet (1998).

[18] U. Egede, PHD Thesis, LUNFD6/(NFFL-7150) (1997).

Figure captions

Fig. 1 Left, E_T distribution of clusters after LVL1 simulation in the EM Calorimeter for events with E_T = 30 GeV electrons and pile-up corresponding to 10^{34} cm^{-2} s^{-1}. On the right, E_T distribution of clusters after LVL1 simulation in the EM Calorimeter for events with jets at both low and high luminosity.

Fig. 2 Left, shower shape in the second compartment of the EM Calorimeter for electrons and jets at low luminosity. Only the LVL1 Trigger was applied beforehand. The distributions are normalised to unit area. Right, difference between the energy found in the second maximum and the energy found in the strip with minimal value in the first compartment of the EM Calorimeter (before any cuts in first compartment). The distributions are shown for electrons and jets at low luminosity for $|\eta| < 1.37$ and are normalised to unit area.

Fig. 3 Angular matching between charged tracks and EM clusters in pseudo-rapidity and azimuth for electrons (dashed) and jets. For the 'jet' sample, various components are shown: electrons from W 's and Z 's (black), electrons from heavy flavour (dense hatch), conversions (light hatch) and hadrons (open). The normalisation between the single electrons and the jet sample is arbitrary.

Fig. 4 Ratio between energy of EM clusters to momentum of reconstructed charged tracks for electrons (dashed) and jets. For the 'jet' sample, various components are shown: electrons from W 's and Z' s (black), electrons from heavy flavour (dense hatch), conversions (light hatch) and hadrons (open). The normalisation between the single electrons and the jet sample is arbitrary.

Fig. 5 E_T distribution for the jet sample at various stages of the analysis both at low and high luminosity. For the 'jet' sample, various components are shown: electrons from W 's and Z 's (black), electrons from heavy flavour (dark hatch), conversions (light hatch) and hadrons (open).

Fig. 6 Cluster E_T distribution for electrons at low and high luminosity for various sets of cuts. 'Reco' here means all the offline cuts.

Fig. 7 Electron efficiency versus η distribution at low and high luminosity for various sets of cuts.

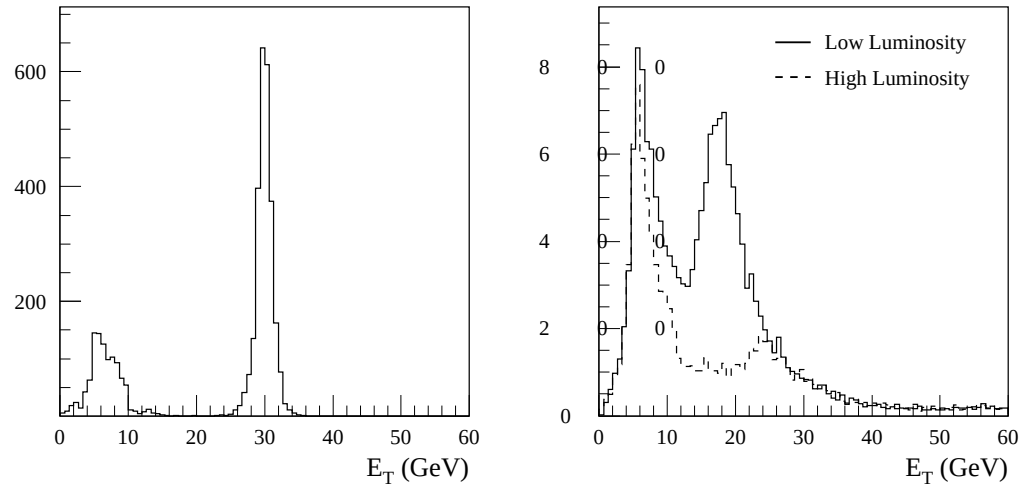

Figure 1:

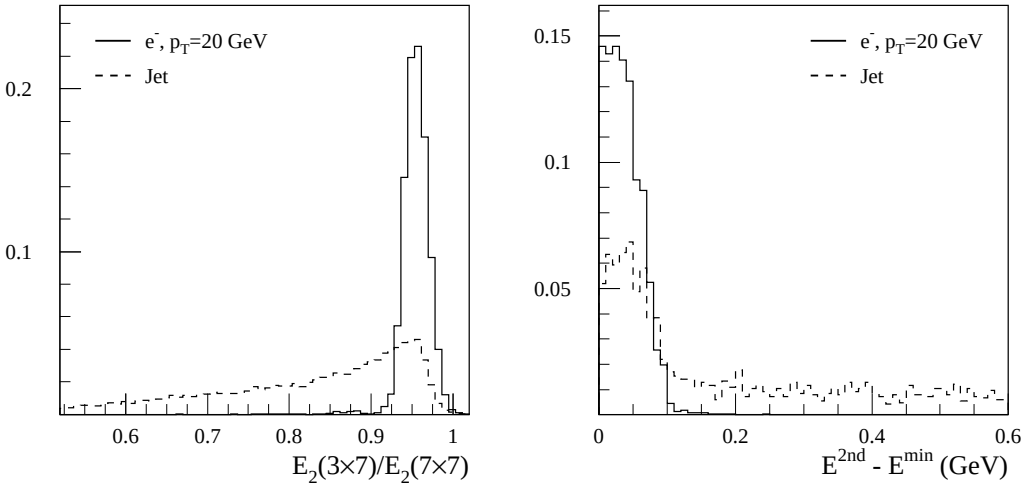

Figure 2:

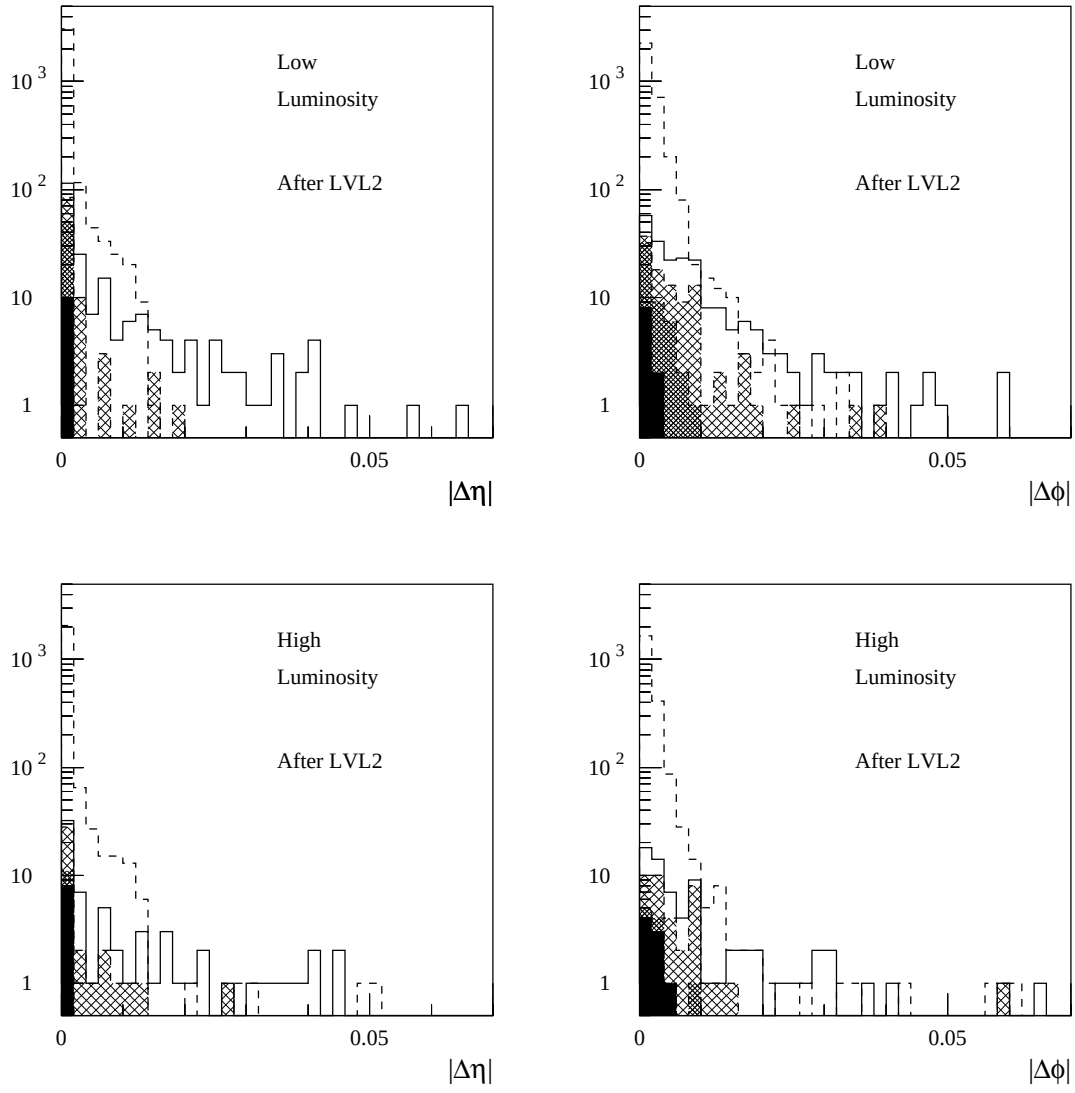
Low
Luminosity
After LVL2
10^3
10^2
10
1
0
0.05
$|\Delta\eta|$
Low
Luminosity
After LVL2
10^3
10^2
10
1
0
0.05
$|\Delta\phi|$
High
Luminosity
After LVL2
10^3
10^2
10
1
0
0.05
$|\Delta\eta|$
High
Luminosity
After LVL2
10^3
10^2
10
1
0
0.05
$|\Delta\phi|$

Figure 3:

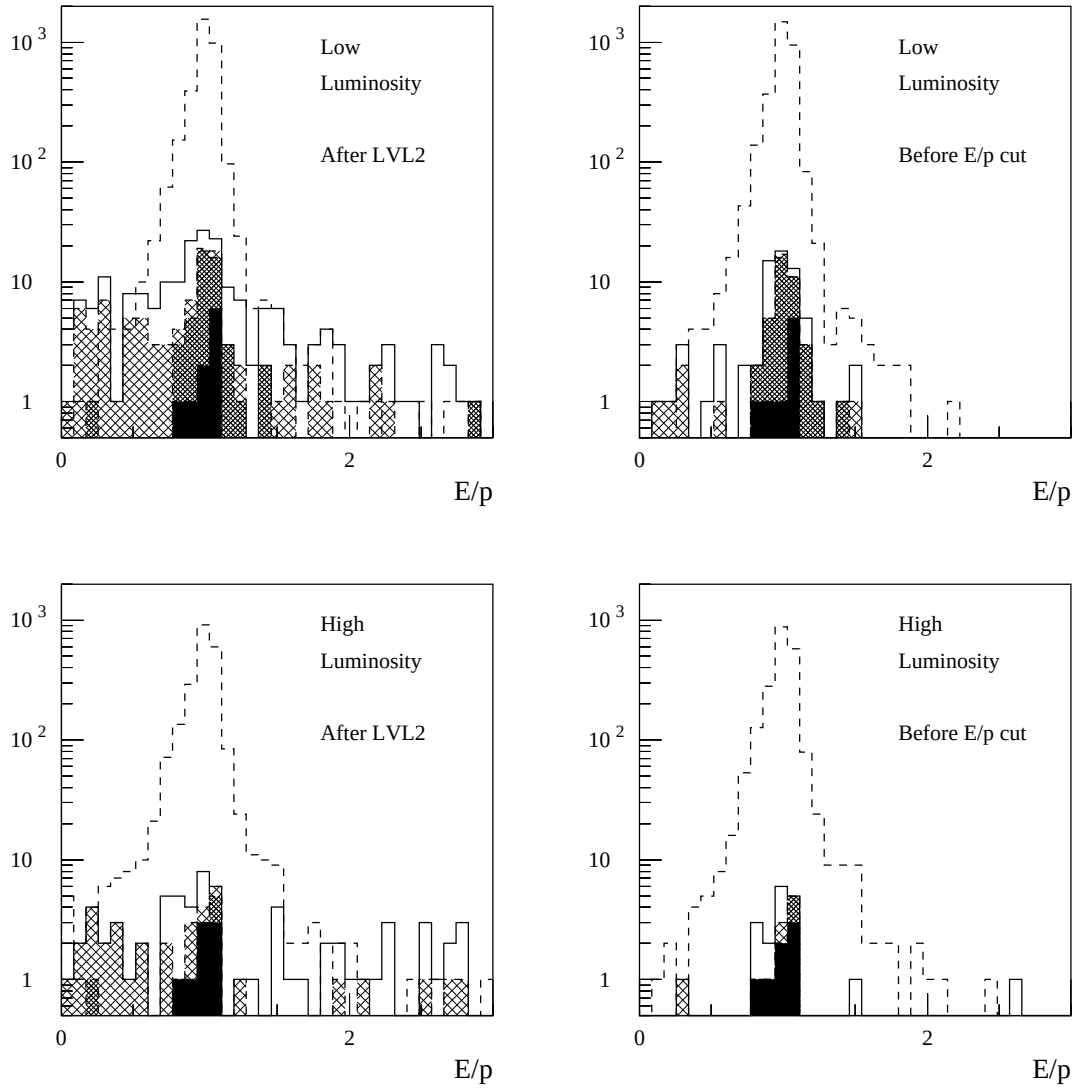
Low
Luminosity
After LVL2
Low
Luminosity
Before E/p cut
High
Luminosity
After LVL2
High
Luminosity
Before E/p cut
E/p

Figure 4:

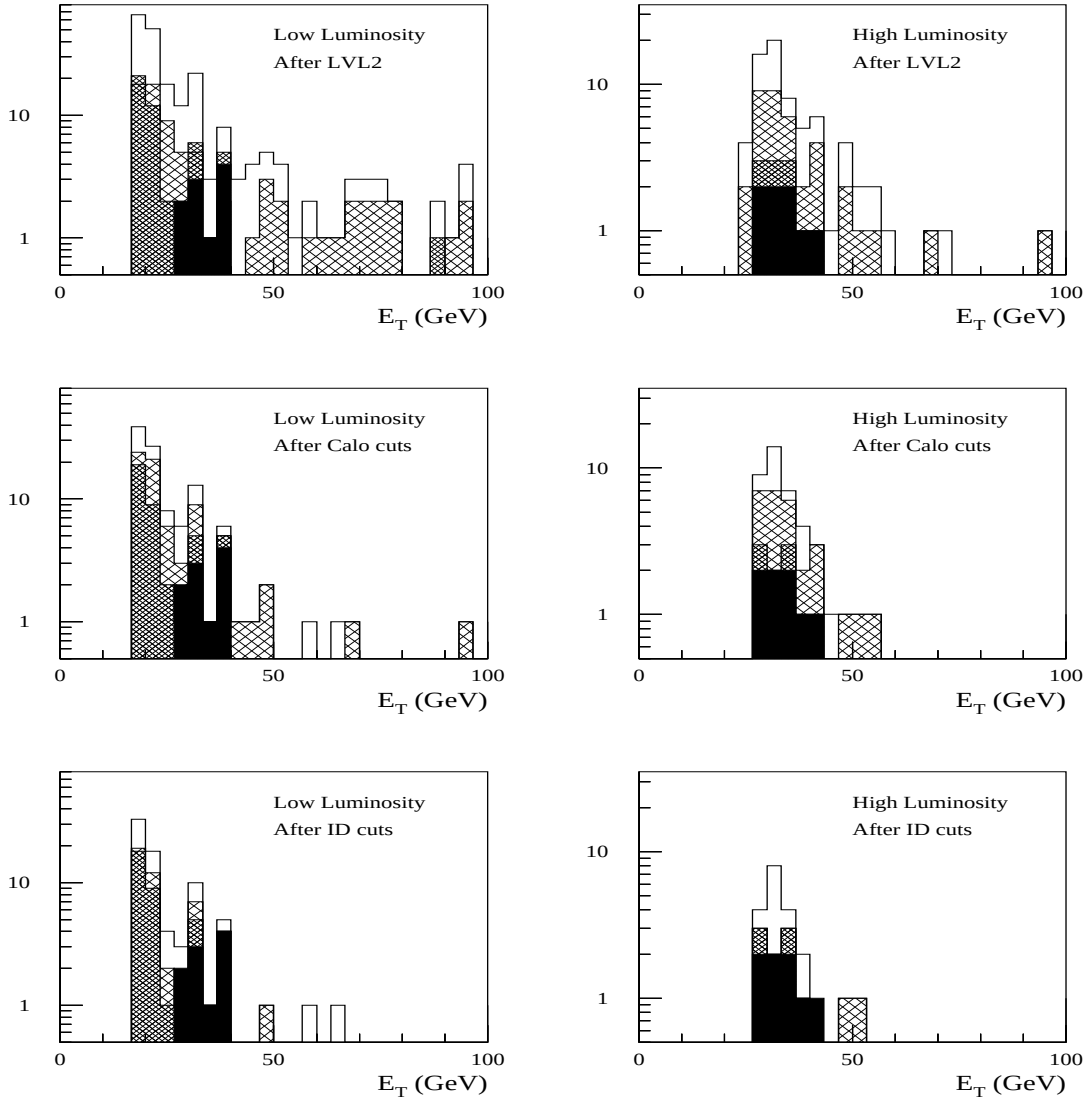
Low Luminosity
After LVL2
High Luminosity
After LVL2
Low Luminosity
After Calo cuts
High Luminosity
After Calo cuts
Low Luminosity
After ID cuts
High Luminosity
After ID cuts
10
1
0
50
100
E_T (GeV)

Figure 5:

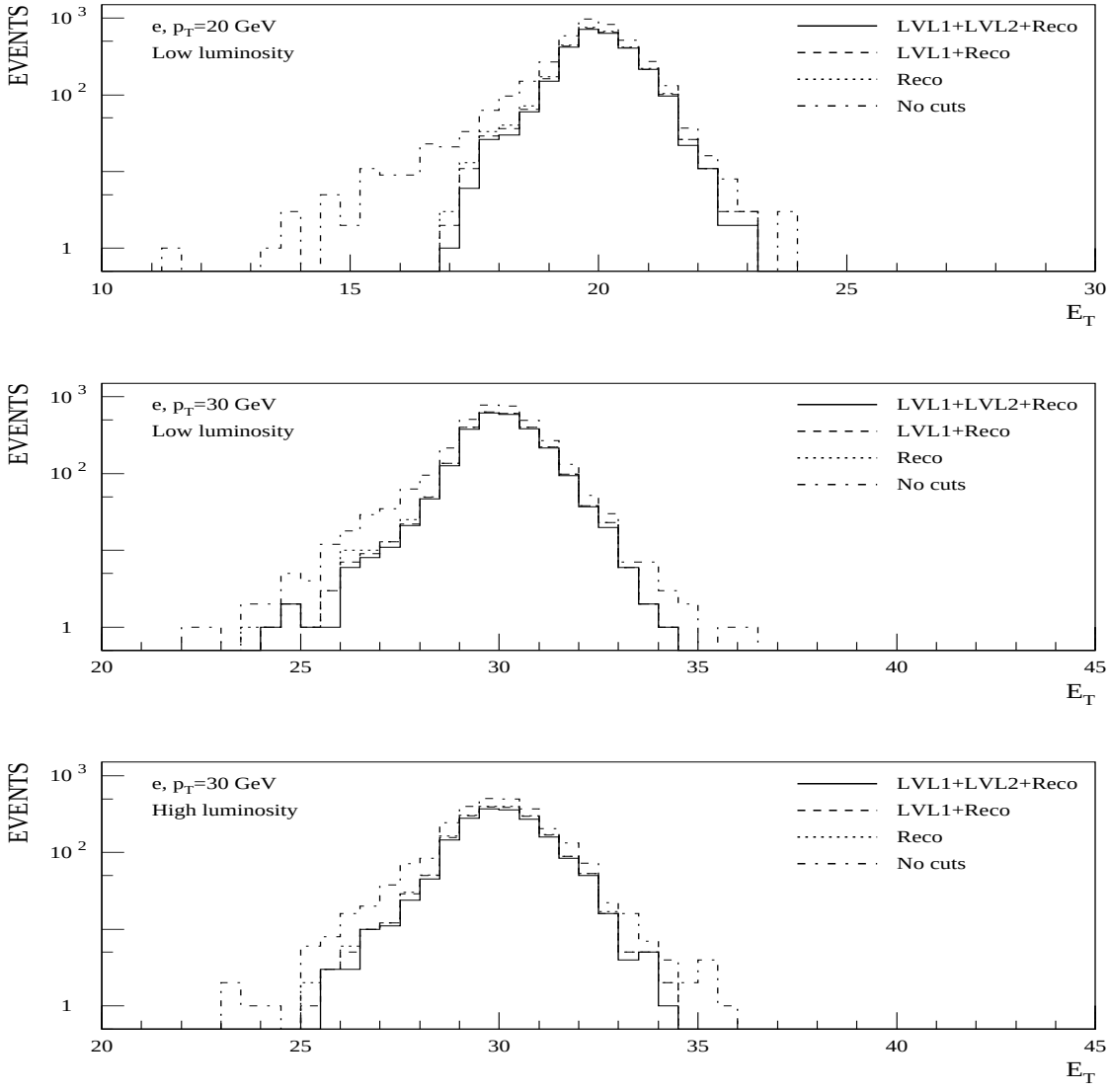
EVENTS
e, p_T=20 GeV
Low luminosity
LVL1+LVL2+Reco
LVL1+Reco
Reco
No cuts
E_T
e, p_T=30 GeV
Low luminosity
LVL1+LVL2+Reco
LVL1+Reco
Reco
No cuts
E_T
e, p_T=30 GeV
High luminosity
LVL1+LVL2+Reco
LVL1+Reco
Reco
No cuts
E_T

Figure 6:

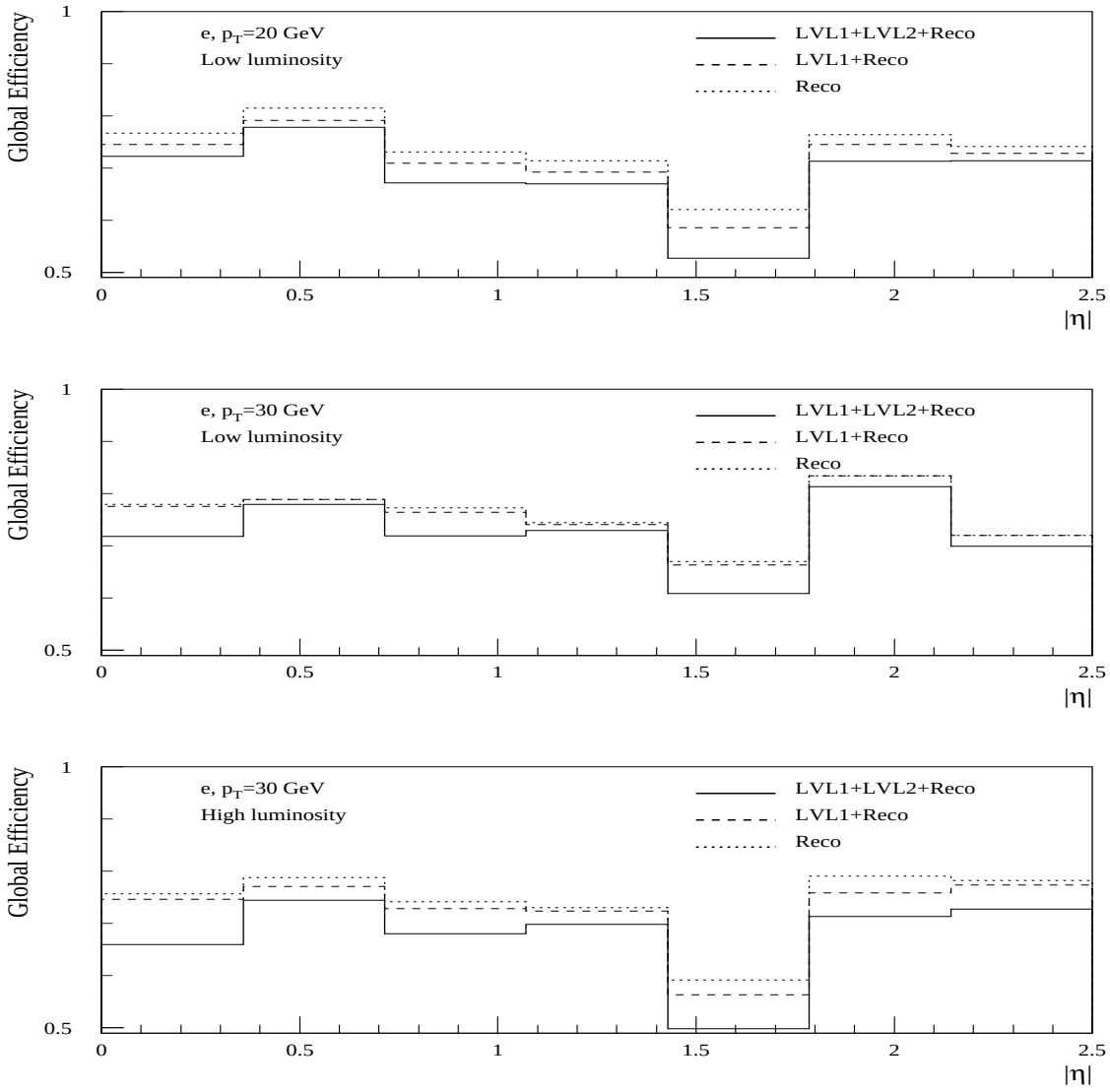
Global Efficiency
1
0.5
e, p_T=20 GeV
Low luminosity
LVL1+LVL2+Reco
LVL1+Reco
Reco
0
0.5
1
1.5
2
2.5
|η|
Global Efficiency
1
0.5
e, p_T=30 GeV
Low luminosity
LVL1+LVL2+Reco
LVL1+Reco
Reco
0
0.5
1
1.5
2
2.5
|η|
Global Efficiency
1
0.5
e, p_T=30 GeV
High luminosity
LVL1+LVL2+Reco
LVL1+Reco
Reco
0
0.5
1
1.5
2
2.5
|η|

Figure 7: